Figure legends

Supplementary Fig. S1

Component of tattoo ink used as reference material was carbon black. (a) SEM image of tattoo ink: uniform particles with diameters of about 40 nm were observed. Scale bar: 100 nm. (b) Raman spectroscopy of tattoo ink and carbon black: tattoo ink showed a Raman shift similar to that of carbon black. D band: defect-induced mode; G band: E2g2 graphite mode. (c) TEM image of tattoo ink and carbon black: Similar particles were observed. Scale bar: 100 nm

Reproduced from reference 35 Hara, K. et al. Evaluation of CNT toxicity in comparison to tattoo ink nanoparticles for use as a biomaterial. Mater Today 14, 434-440, 2011, with permission.

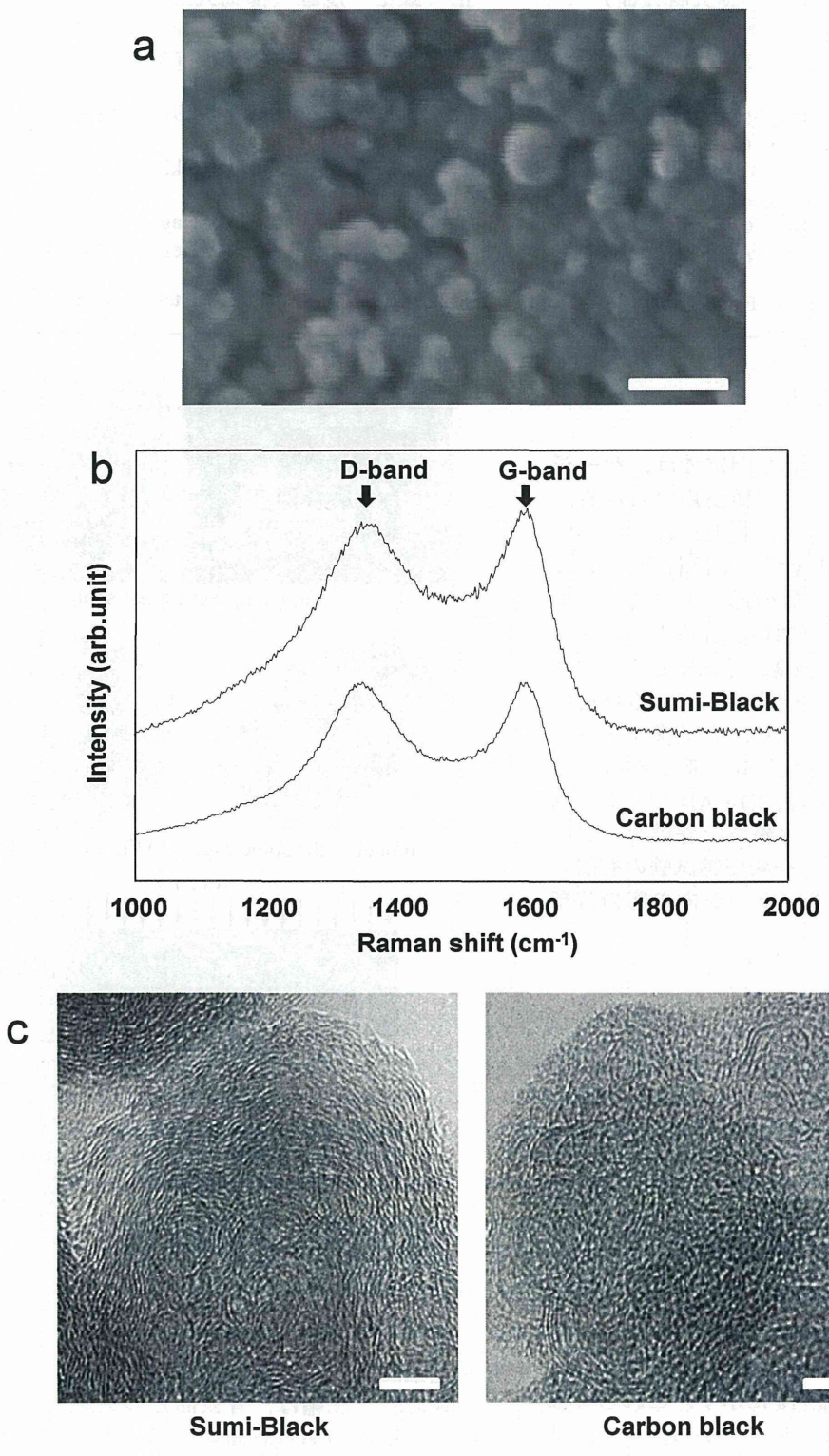

Supplementary Fig. S1

4H1　一軸圧縮試験における脊椎ケージの有限要素応力解析

Finite element analysis of spine cage in the uniaxial compression test

○正　大澤　恭子（福岡大材技研）　　正　森山　茂章（福岡大工）
非　湯谷　知世（ナカシマメディカル）　非　西村　直之（ナカシマメディカル）
非　薄井　雄企（信州大工）　　非　齋藤　直人（信州大医）

Takako OSAWA, Institute of Materials Science and Technology, Fukuoka University, 8-19-1, Nanakuma, Fukuoka
Shigeaki MORIYAMA, Department of Mechanical Engineering, Fukuoka University
Tomoyo YUTANI, Nakashima Medical CO., LTD., R&D Center, 5322, Haga, Kita-ku, Okayama
Naoyuki NISHIMURA, Nakashima Medical CO., LTD., R&D Center
Yuki USUI, Research Center for Exotic Nanocarbons, Shinshu University, Matsumoto, Nagano
Naoto SAITO, Department of Applied Physical Therapy, Shinshu University School of Health Sciences

Key Words: Spine Cage, Finite element analysis, Stress distribution, Uniaxial compression test, 3D-CAD

1. はじめに

多くの脊椎手術で行われる脊椎固定では，ケージを含む脊椎椎体スペーサーと骨移植が用いられる．従来これらに使用されるチタンは骨と比較して剛性が高く，母床の脊椎椎体が圧潰する危険性がある [1]．近年，金属材に比べて弾性係数の低いポリエーテルエーテルケトン（PEEK）材が頻用されるようになった．PEEK 材料は高い機械的強度，寸法安定性，耐薬品性に優れており，脊椎スペーサーに用いる材料として十分な力学特性を有している．脊椎椎体スペーサーである脊椎ケージのような複雑な形状を有するインプラントの力学的評価では，3D-CAD データに基づく数値解析が有効である．本報では脊椎ケージの 3D-CAD 形状データに基づき，一軸圧縮試験の有限要素シミュレーションを実行し，ケージ内の応力分布を評価した．

2. 方法

脊椎ケージ圧縮試験の力学解析は，脊柱ケージおよび固定治具の 3D-CAD 形状データを汎用有限要素解析ソフト Abaqus (ver6.11, SIMULIA) に読み込み実行した．3D-CAD から Abaqus への形状データの受け渡しは，CAD システム間で相互にグラフィックのやり取り可能な中間データ形式である IGES 形式で行った．PEEK 製の箱型脊椎ケージを，その形状に合わせた ポリフェニルサルフォン（PPSU）製の固定治具で挟んだ一軸圧縮試験を有限要素解析によりシミュレートした．

対象の圧縮試験機構を Fig. 1a に示す．これら脊椎ケージと固定治具の 3D-CAD データから，ケージは 10 節点四面体要素，治具は 8 節点六面体要素にそれぞれ離散化した．ケージおよび治具の有限要素モデルを Fig. 1b, c に示す．

圧縮試験の境界条件（Fig.1d）は，下方治具の下面を完全固定し，上方治具の上面に 3375 N の圧縮力を負荷した．圧縮は，骨表面とのアンカリングのための波状突起のある表面を上面および底面とした軸方向に沿って与えた．脊椎ケージと固定治具のアセンブリにおいて，ケージと治具が接する領域を接触表面とし，接触相互作用特性として摩擦係数 0.2 の接触条件を設定した．

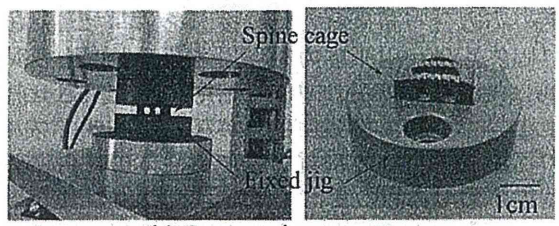

(a) Compression test setup

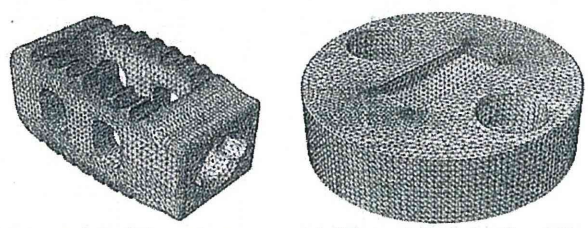
(b) FE model of the spine cage　(c) FE model of the fixed jig

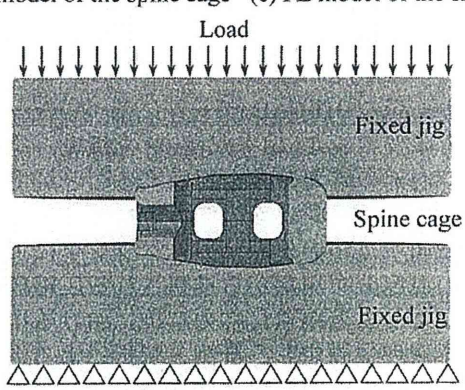

(d) Boundary conditions (Cross-section)

Fig. 1 Finite element analysis of the spine cage in the compression test.

解析対象の材料特性として，ケージと治具はともに等方線形弾性体と仮定した．脊柱ケージの材料特性は，純 PEEK の物性値を参考にヤング率 3368 MPa，ポアソン比 0.4 を与えた．治具の材料特性は，PPSU の物性値を参考にヤング率 2300 MPa，ポアソン比 0.4 を与えた．

3. 結果と考察

脊椎ケージ表面の相当応力分布を Fig. 2 に示す．脊椎ケージにおいて，上面および底面の波状突起部分と側面の貫通孔内側に応力の集中が見られた．

得られた応力解析結果の妥当性を評価するために，温度と応力の比例関係を表す熱弾性論に基づき，赤外線サーモグラフィで計測したサンプル表面の温度分布から求めた応力測定結果と，解析によるケージ表面の応力分布結果との比較検討を試みた．対象物体（固体）に，引張応力を作用させると応力変動に比例した温度降下が，逆に圧縮応力を作用させれば温度上昇を生じる熱弾性現象が起きる．サンプル表面の温度変化は等方均質な線形弾性体の材料においては主応力の総和の変化量に比例する [2]．圧縮試験機構の脊柱ケージ表面の温度分布と，解析によって求められた主応力の総和の分布図を Fig. 3 に示す．赤外線サーモグラフィ計測では側面の貫通孔内側に温度の上昇がみられたことから，当該部位では圧縮が働いていると推察される．解析結果においてケージ貫通孔内側での主応力の総和では圧縮が見られ，赤外線サーモグラフィによる温度分布測定から推察される応力と，圧縮部位が一致した．

4. おわりに

脊椎ケージの 3D-CAD データに基づいた一軸圧縮試験の有限要素シミュレーションを行い，ケージ表面および内部の応力分布を評価することができた．得られた脊椎ケージ表面の応力分布において圧縮が見られた領域は，赤外線サーモグラフィによるケージ表面の温度分布測定から推察される圧縮箇所が一致した．このことから，応力解析における接触・拘束条件を適切に設定し，計測と解析による応力分布の整合性を向上させれば，赤外線カメラの視野内に入っていないケージ上面および底面の波状突起部分などケージ-治具接触領域や構造物内部の応力に対し，FE 解析を通して評価できる可能性が示唆された．

謝　辞

本研究の一部は，厚生労働科学研究費補助金の助成を受けたものである．赤外線サーモグラフィによる応力測定では，JFE テクノリサーチ株式会社の森田智之氏と渋谷清氏のご協力のもとで実施された．ここに謝意を表します．

Fig. 2 von Mises stress distribution of the spine cage

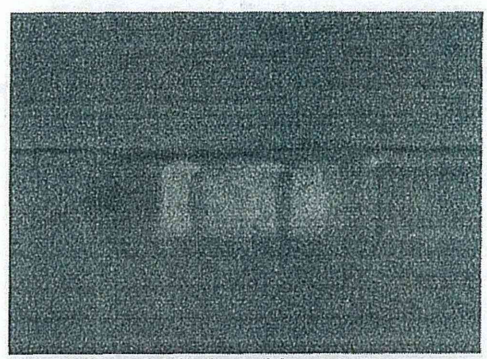

(a) Infrared image

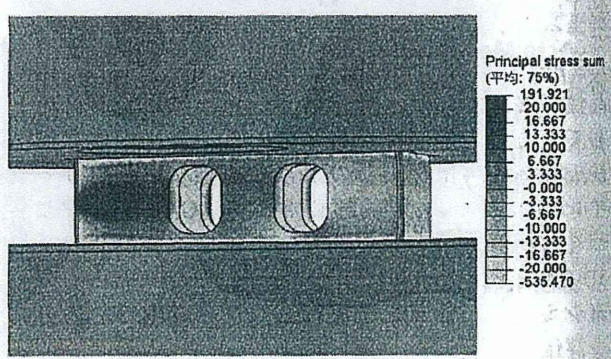

(b) Principal stress sum

Fig. 3 Infrared thermography image and principal stress sum distribution over the spine cage of compression test setup

文 献

1) 松下富春　他，チタン多孔体を用いた脊椎固定術用椎間スペーサーの開発，生命健康科学研究所紀要，No. 5（2009）pp.20-29.

2) 西名慶晃，今西大輔，渋谷清，高精度赤外線サーモグラフィを活用した各種測定技術（温度・応力・疲労・亀裂）とその応用，JFE 技報 No. 27,（2011）p. 9-14.

Effects of CNT waviness on the effective elastic responses of CNT-reinforced polymer composites

K. Yanase, S. Moriyama & J. W. Ju

Acta Mechanica

ISSN 0001-5970
Volume 224
Number 7

Acta Mech (2013) 224:1351-1364
DOI 10.1007/s00707-013-0808-3

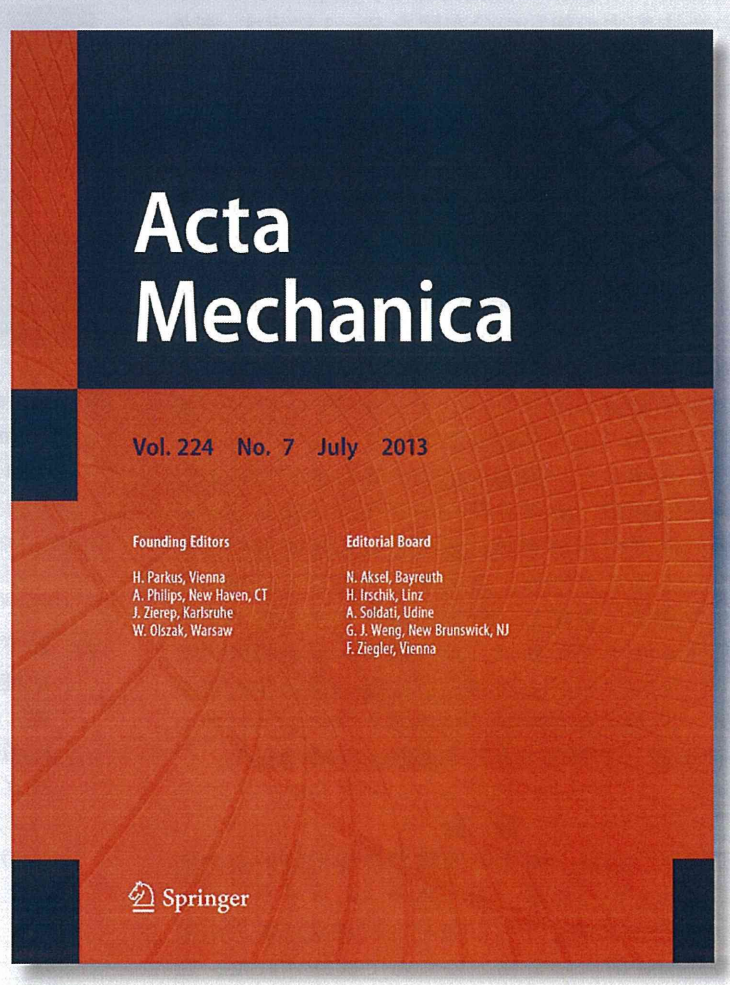

Springer

Acta Mech 224, 1351–1364 (2013)
DOI 10.1007/s00707-013-0808-3

K. Yanase · S. Moriyama · J. W. Ju

Effects of CNT waviness on the effective elastic responses of CNT-reinforced polymer composites

Received: 17 October 2012 / Revised: 12 December 2012 / Published online: 30 January 2013

Abstract In this study, the effects of fiber waviness on the effective elastic responses of CNT–polymer composites are investigated based on the framework of micromechanics and homogenization. By taking advantage of an ad hoc Eshelby tensor, the load-transfer capability of wavy carbon nanotube (CNT) embedded in the polymer matrix is accounted for. Further, the effective elastic responses of composites are simulated by using the multi-phase Mori–Tanaka method to study the influence of randomly oriented wavy CNT. It is demonstrated that the proposed micromechanics-based closed form solution is effective to tackle the underlying problem. The present predictions and the comparisons with the available experimental data indicate that the CNT waviness leads to the degradation of effective responses of composites. Finally, in addition to the effect of CNT waviness, the significance of CNT interface is briefly discussed based on the experimental observations.

1 Introduction

For applications where weight, stiffness, and strength are critical, polymers reinforced with carbon nanotubes (CNTs) offer the potential for significant improvement over systems such as graphite fiber-reinforced polymers. Other potential advantages of CNT–polymer composites include multifunctionality, increased energy absorbance, improved toughness, and ease of manufacturing [1]. Therefore, CNT–polymer composites have been increasingly studied due to their attractive properties and potential for a wide range of applications. CNTs are predicted to have modulus values on the order of 1 TPa, with strengths several times that of graphite fibers. Given the significance of the CNT's mechanical properties, substantial improvement on current composites should be possible by exploiting the CNT's unique characteristics exhibited at the nanoscale and the macroscale levels. In practice, a better understanding of the relationship between processing, interfacial optimization, morphology, and composite properties is a major goal of this area of research. This may lead to optimal reinforcement of polymer matrices with CNTs [2].

Much of the research on the preparation of CNT–polymer composites has been driven by a desire to exploit the tube's stiffness and strength. Even when the interest has been focused on other properties, the ability of nanotubes to improve the mechanical characteristics of a polymer has often been a valuable added benefit.

K. Yanase (✉) · S. Moriyama
Department of Mechanical Engineering, Institute of Materials Science and Technology,
Fukuoka University, Fukuoka City, Fukuoka 814-0180, Japan
E-mail: kyanase@fukuoka-u.ac.jp

S. Moriyama
E-mail: moriyama@fukuoka-u.ac.jp

J. W. Ju
Department of Civil and Environmental Engineering, University of California Los Angeles, CA 90095-1593, USA
E-mail: juj@ucla.edu

In early work, the measured properties were often disappointing, but such studies were of value in understanding the reasons for composite failure and in identifying the critical issues that need to be addressed. For example, it was reported that the observed curvature of embedded CNTs or waviness significantly reduced their reinforcement capabilities compared to straight CNTs [2]. It was also noted that other indistinguishable factors can contribute to the low values measured in experimental data, including weak interfacial bonding, insufficient dispersion, the nature of interaction between the polymer and CNTs, the size, shape, and orientation of CNTs, the type of CNTs employed (single-wall, multi-wall, bundles, etc.), and degradation of the CNTs due to processing.

As a result of their very small diameters, CNTs are very flexible and therefore often observed to be curled and looped rather than straight [3]. It is well recognized, based on numerous research on micro-fiber-reinforced composites, that fiber-matrix interfacial shear stress is a critical parameter in controlling the efficiency of load transfer. This significantly affects the mechanical properties of composites such as the elastic modulus, tensile strength, and fracture toughness. Therefore, anticipated potential applications of CNT-reinforced composites demand a better understanding of the CNT-matrix interfacial characteristics [2–7]. Moreover, at present, uniform distribution of CNTs within the matrix remains a challenging task in the fabrication process [8,9]. In practice, the reinforcing effect of the CNT agglomerate is countervailed by the fact that they also act as flaws or stress concentration sites within the composites. The degradation of failure strain and tensile strength associated with increase in CNT content suggests that CNTs are not well dispersed in the matrix. Accordingly, the homogeneity of the composite is a critical issue for the mechanical behavior of composites [4,7,9,10].

In nanocomposites, the interactions between the CNTs and the matrix take place at the nanoscale level, but they affect the mechanical response of composites at the macroscopic level. Nanoscale phenomena are often studied by molecular dynamics (MD) simulations while the behavior at the macroscopic level is conveniently studied with continuum mechanics. MD simulations are limited only to small volumes because of the intensive computational requirements. Nanocomposites for engineering applications expand from nano to micro and eventually to macro length scale, which must be addressed by other simulation approaches or combination of MD with other approaches [11].

Continuum approaches based on continuum mechanics have also been applied successfully to simulate the macroscopic responses of CNT-reinforced composites. The analytical models based on Eshelby's equivalence principle [12] aim at the analysis of a representative volume element (RVE) or representative area element (RAE) in which the reinforcements are randomly distributed. The main advantage of Eshelby's approach is that it enables us to predict the full multi-axial properties and responses of heterogeneous materials, which are often difficult to measure experimentally. In the literatures, Eshelby's approach has been extensively used to predict the effective mechanical properties of composites (e.g., [13–25]). Concerning the CNT-reinforced composites, Fisher et al. [1,26] and Bradshaw et al. [27] adopted the FE analysis and the micromechanical framework [14,15] to examine the influence of CNT waviness on the reinforcing capability of CNT and the effective elastic properties of composites. In the literatures, the benefit of utilizing CNTs to improve the yield strength of a material has not been adequately addressed. However, the low density, high stiffness, and high tensile strength of CNT can make it a truly attractive reinforcing agent not just for its elastic stiffness. Correspondingly, Barai and Weng [9] proposed a two-scale micromechanics model to investigate the effects of the CNT agglomeration and the imperfect interface condition (cf. [28–31]) upon the elastoplastic behavior of composites.

To promote our understanding of new materials such as CNT–polymer composites, it is useful to develop models to simulate the effective properties of those materials. An effective mean to accomplish this is the extension of traditional micromechanics and composite models that can address distinct characteristic of the materials. Accordingly, in this study, the effects of CNT waviness on the effective elastic responses of CNT–polymer composites are investigated in the framework of micromechanics and homogenization. By taking advantage of an ad hoc Eshelby tensor, the micromechanical field equations are systematically presented. Based on a series of parametric studies, the significance of CNT waviness is examined. Finally, in addition to the effects of CNT waviness, the importance of the CNT interface is briefly discussed based on the experimental observations.

2 Effective elastic responses of wavy CNT-reinforced polymer composites

2.1 Load-transfer capability of wavy CNT

Based on the Mori–Tanaka method [14,15,30], the effective stiffness of a composite is given as:

$$\mathbf{C}^* = \mathbf{C}^0 \bullet \left\{ \mathbf{I} + \phi \left[(\mathbf{C}^1 - \mathbf{C}^0)^{-1} \bullet \mathbf{C}^0 + (1-\phi)\mathbf{S} \right]^{-1} \right\} \tag{1}$$

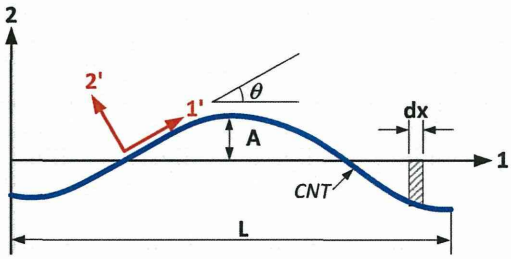

Fig. 1 Representation of fiber waviness [33]

where $\mathbf{C}^0$ and $\mathbf{C}^1$ are the fourth-order elastic stiffness of the matrix and CNT, respectively; $\mathbf{I}$ is the fourth-order identity tensor; ϕ is the volume fraction of CNT. Further, to represent the high aspect ratio (length/diameter) of CNT, the Eshelby tensor $\mathbf{S}$ for a long circular fiber is adopted in Eq. (1) as follows (cf. [30,32]):

$$S_{1111} = S_{1122} = S_{1133} = 0; \quad S_{2222} = S_{3333} = \frac{5 - 4\nu_0}{8(1 - \nu_0)}; \quad S_{2211} = S_{3311} = \frac{\nu_0}{2(1 - \nu_0)}; \tag{2}$$

$$S_{2233} = S_{3322} = \frac{4\nu_0 - 1}{8(1 - \nu_0)}; \quad S_{1212} = S_{1313} = \frac{1}{4}; \quad S_{2323} = \frac{3 - 4\nu_0}{8(1 - \nu_0)}, \tag{3}$$

where ν_0 signifies Poisson's ratio of the matrix. It is worth noting some simplifications made in the model. First, treating the inclusion as a solid cylinder neglects the hollow nature of CNT. Second, the specific form of CNT (SWNT, MWNT, or NT bundle) is disregarded. Finally, any possible relative motion between the individual shells or tubes in a MWNT and NT bundle is not taken into account [1].

For unidirectional fiber-reinforced composites, fiber waviness is a manufacturing defect occurring especially during the filament winding process. Layer waviness also occurs in thick cross ply or multi-directional laminates due to the lamination residual stress built up during curing. In the literature, the analytical study aiming for prediction of the major Young's modulus of wavy composites was conducted by Hsiao and Daniel [33]. In this research, the analytical approach by Hsiao and Daniel [33] is incorporated into the micromechanical framework to investigate the effects of CNT waviness. Accordingly, it is assumed that the fiber waviness of CNT is planar sinusoidal (Fig. 1):

$$v = A \sin \frac{2\pi x}{L}, \tag{4}$$

where A and L represent the amplitude and the length of the wavy fiber, respectively. By applying the successive coordinate transformation, the stiffness of wavy-fiber-reinforced composite can be evaluated by the following integral equation (Fig. 1):

$$\bar{C}_{ijkl} = \frac{1}{L} \int_0^L Q_{ip} Q_{jq} Q_{kr} Q_{ls} C^*_{pqrs} \mathrm{d}x, \quad \text{where} \quad Q_{ij} = \begin{bmatrix} \cos\theta & -\sin\theta & 0 \\ \sin\theta & \cos\theta & 0 \\ 0 & 0 & 1 \end{bmatrix}. \tag{5}$$

To average the properties over the length of a fiber, it is necessary to relate angle θ to the wave parameters A and L as follows [33]:

$$m = \cos\theta = \left[1 + \left(2\pi \frac{A}{L} \cos \frac{2\pi x}{L}\right)^2\right]^{-1/2}, \tag{6}$$

$$n = \sin\theta = 2\pi \frac{A}{L} \cos \frac{2\pi x}{L} \left[1 + \left(2\pi \frac{A}{L} \cos \frac{2\pi x}{L}\right)^2\right]^{-1/2}. \tag{7}$$

Subsequently, the integrals in Eq. (5) can be explicitly calculated as:

$$\frac{1}{L} \int_0^L m^4 \mathrm{d}x = \frac{2 + \alpha^2}{2(1 + \alpha^2)^{3/2}} = I_1; \quad \frac{1}{L} \int_0^L m^2 n^2 \mathrm{d}x = \frac{\alpha^2}{2(1 + \alpha^2)^{3/2}} = I_2, \tag{8}$$

$$\frac{1}{L}\int_0^L m^2 \mathrm{d}x = \frac{1}{(1+\alpha^2)^{1/2}} = I_1 + I_2; \quad \frac{1}{L}\int_0^L n^2 \mathrm{d}x = 1 - \frac{1}{(1+\alpha^2)^{1/2}} = 1 - I_1 - I_2, \tag{9}$$

$$\frac{1}{L}\int_0^L n^4 \mathrm{d}x = 1 - \frac{2+3\alpha^2}{2(1+\alpha^2)^{3/2}} = 1 - I_1 - 2I_2, \tag{10}$$

$$\frac{1}{L}\int_0^L m^3 n \mathrm{d}x = \frac{1}{L}\int_0^L m n^3 \mathrm{d}x = \frac{1}{L}\int_0^L m^3 n \mathrm{d}x = \frac{1}{L}\int_0^L mn \mathrm{d}x = 0, \tag{11}$$

where

$$\alpha = 2\pi \frac{A}{L}. \tag{12}$$

Accordingly, the components in Eq. (5) can be explicitly expressed as:

$$\bar{C}_{1111} = I_1 \left(C^*_{1111} - C^*_{2222}\right) + 2I_2 \left(C^*_{1122} - C^*_{2222} + 2C^*_{1212}\right) + C^*_{2222}, \tag{13}$$

$$\bar{C}_{1122} = I_2 \left(C^*_{1111} - 2C^*_{1122} + C^*_{2222} - 4C^*_{1212}\right) + C^*_{1122}, \tag{14}$$

$$\bar{C}_{1133} = I_1 \left(C^*_{1122} - C^*_{2233}\right) + I_2 \left(C^*_{1122} - C^*_{2233}\right) + C^*_{2233}, \tag{15}$$

$$\bar{C}_{2211} = I_2 \left(C^*_{1111} - 2C^*_{1122} + C^*_{2222} - 4C^*_{1212}\right) + C^*_{1122}, \tag{16}$$

$$\bar{C}_{2222} = I_1 \left(C^*_{2222} - C^*_{1111}\right) + I_2 \left(2C^*_{1122} + 4C^*_{1212} - 2C^*_{1111}\right) + C^*_{1111}, \tag{17}$$

$$\bar{C}_{2233} = I_1 \left(C^*_{2233} - C^*_{1122}\right) + I_2 \left(C^*_{2233} - C^*_{1122}\right) + C^*_{1122}, \tag{18}$$

$$\bar{C}_{3311} = (I_1 + I_2) \left(C^*_{1122} - C^*_{2233}\right) + C^*_{2233}, \tag{19}$$

$$\bar{C}_{3322} = (I_1 + I_2) \left(C^*_{2233} - C^*_{1122}\right) + C^*_{1122}, \tag{20}$$

$$\bar{C}_{3333} = C^*_{3333}, \tag{21}$$

$$\bar{C}_{1212} = I_2 \left(C^*_{1111} - 2C^*_{1122} + C^*_{2222} - 4C^*_{1212}\right) + C^*_{1212}, \tag{22}$$

$$\bar{C}_{2323} = (I_1 + I_2) \left(C^*_{2323} - C^*_{1212}\right) + C^*_{1212}, \tag{23}$$

$$\bar{C}_{1313} = (I_1 + I_2) \left(C^*_{1212} - C^*_{2323}\right) + C^*_{2323}. \tag{24}$$

The effective longitudinal Young's modulus in the 1-direction, $\bar{E}_1$, is given as:

$$\bar{E}_1 = \frac{1}{\bar{D}_{1111}}, \quad \text{where} \quad \bar{\mathbf{D}} = \bar{\mathbf{C}}^{-1}. \tag{25}$$

Based on Eq. (25) and a simple volume summation, the reinforcing capability of wavy CNT is evaluated by the following equation ([1,26,34]):

$$E_{\text{wavy}} = \lim_{\phi \to 0} \frac{\bar{E}_1 - (1-\phi)E^0}{\phi}. \tag{26}$$

Figure 2 shows the variations of E_{wavy} associated with the waviness factor, $w = A/L$. As clearly displayed, the fiber waviness significantly lowers the effectiveness of CNT. The present analysis tends to estimate higher modulus compared to the FEM analysis [26] in particular for $E^1/E^0 = 1,000$ as exhibited by Fig. 2a. Further, Fig. 2b illustrates the extent of relative degradation, E_{wavy}/E^1, and the present analysis is relatively insensitive to the value of E^1/E^0. The obtained result in Fig. 2a is similar to the result reported by Anumandla and Gibson [34].

To reproduce Eq. (5) with the Mori–Tanaka method, we substitute $\mathbf{C}^* = \bar{\mathbf{C}}$ and $\mathbf{S} = \bar{\mathbf{S}}$ in Eq. (1) as follows:

$$\bar{\mathbf{C}} = \mathbf{C}^0 \bullet \left\{\mathbf{I} + \phi \left[(\mathbf{C}^1 - \mathbf{C}^0)^{-1} \bullet \mathbf{C}^0 + (1-\phi)\bar{\mathbf{S}}\right]^{-1}\right\}. \tag{27}$$